Electronic Supplementary Information for

Enhancing Photovoltaic Performance by Tuning the Disc-Shaped Aggregated Domain Sizes of a Chlorinated-Small-Molecule Acceptor and Side-Chain-Engineered Fluorinated-Conjugated Polymer Donors

Yu-Che Lin,[a] *Yi-Ju Lu,*[a] *Cheng-Si Tsao,*[b,c] *Akinori Saeki,*[d] *Jia-Xing Li,*[e] *Chung-Hao Chen,*[a] *Hao-Cheng Wang,*[a] *Hsiu-Cheng Chen,*[a] *Dong Meng,*[f] *Kaung-Hsiung Wu,*[e] *Yang Yang,*[f] *and Kung-Hwa Wei**[a,g]

[a]Department of Materials Science and Engineering, National Chiao Tung University, Hsinchu 30010, Taiwan
[b]Department of Materials Science and Engineering, National Taiwan University, Taipei 10617, Taiwan
[c]Institute of Nuclear Energy Research, Taoyuan 32546, Taiwan
[d]Department of Applied Chemistry, Graduate School of Engineering, Osaka University, 2-1 Yamadaoka, Suita, Osaka 565-0871, Japan
[e]Department of Electrophysics, National Chiao Tung University, Hsinchu 30010, Taiwan
[f]Department of Material Science and Engineering, University of California, Los Angeles, CA 90095, USA
[g]Center for Emergent Functional Matter Science, National Chiao Tung University, Hsinchu 30010, Taiwan

***Corresponding Author**
khwei@mail.nctu.edu.tw

Materials and Synthesis

4,7-Bis(5-bromothien-2-yl)-5,6-bis(octyloxy)benzo[*c*][1,2,5]oxadiazole (**M1**), 7-bis(5-bromothien-2-yl)-5,6-bis(2-ethylhexyloxy)benzo[*c*][1,2,5]oxadiazole (**M2**), and (4,8-bis(4-fluoro-5-(2-ethylhexyl)thien-2-yl)benzo[1,2-*b*:4,5-*b*´]dithiophene-2,6-diyl)bis(trimethylstannane) (**M3**) were prepared according to reported procedures.[1,2]

General Procedure for Stille Polymerization: **Alternating Polymer BO2FC8. M1** (42.6 mg, 0.061 mmol), **M2** (57.4 mg, 0.061 mmol), and tri-*o*-tolylphosphine (1.5 mg, 8.0 mol %) were dissolved in dry chlorobenzene (CB, 2 mL) and degassed for 15 min. $Pd_2(dba)_3$ (1.12 mg, 2.0 mol %) was dissolved in dry CB and added in one portion under N_2, and then the mixture was heated at 130 °C for 60 h. The hot solution was added dropwise into MeOH (50 mL). The solid was filtered through a Soxhlet thimble and washed with MeOH, acetone, hexane, and $CHCl_3$ in a Soxhlet apparatus. The $CHCl_3$ solution was concentrated and then added dropwise into MeOH. The crude polymer was collected, dissolved in $CHCl_3$, and reprecipitated from MeOH. The precipitate was collected and dried under vacuum to give **BO2FC8** (60 mg, 85%). Anal. Calcd: C, 66.63; H, 6.81; N, 2.43. Found: C, 66.36; H, 6.72; N, 2.38.

BO2FEH (54 mg, 77%) Anal. Calcd: C, 66.63; H, 6.81; N, 2.43. Found: C, 66.71; H, 6.64; N, 2.36.

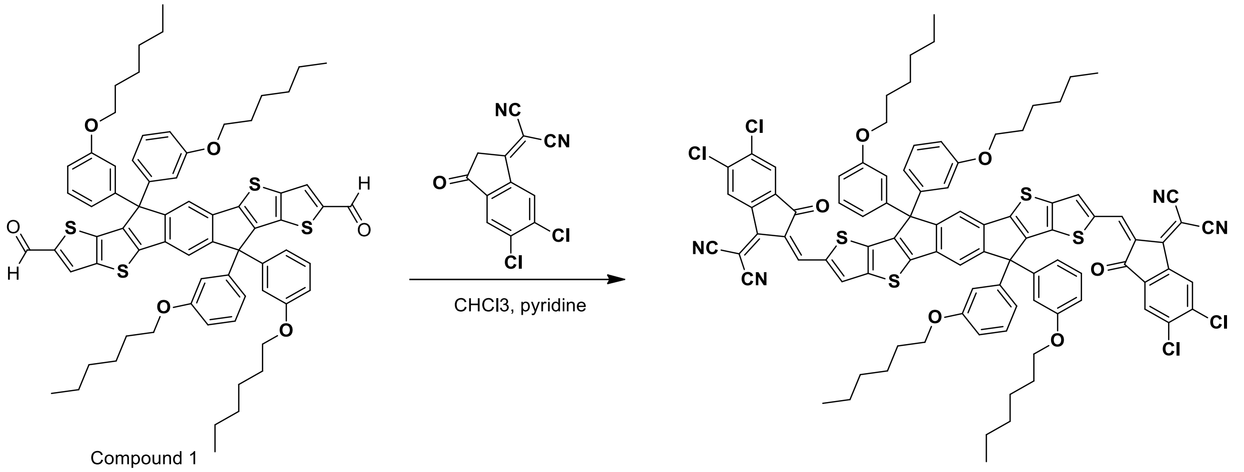

Compound 1

Scheme S1. Synthesis of m-ITIC-OR-4Cl.

m-ITIC-OR-4Cl

Compound **1** (**Scheme S1**)[3] (114 mg, 0.100 mmol) and 2-(5,6-dichloro-3-oxo-2,3-dihydro-1*H*-inden-1-ylidene)malononitrile[4] (132 mg, 0.500 mmol) were dissolved in $CHCl_3$ (100 mL) under N_2 and then pyridine (1 mL) was added. The mixture was heated under reflux overnight. After cooling to room temperature, the mixture was loaded directly onto a short column of silica gel and eluted with CH_2Cl_2. The crude compound was purified again through another silica gel column, eluting with CH_2Cl_2/hexane, to give a black solid (121 mg, 74%) ^1H NMR ($CDCl_3$, 300 MHz), δ (ppm): 8.896 (s, 2H), 8.768 (s, 2H), 8.174 (s, 2H), 7.883 (s, 2H), 7.663 (s, 2H), 7.204 (d, 4H), 6.824–6.874 (m, 12H), 3.918–4.002 (m, 8H), 1.711–1.760 (m, 8H), 1.258–1.306 (m, 24H), 0.842 (t, 12H). ^{13}C NMR ($CDCl_3$, 300 MHz), δ (ppm): 159.52, 147.77, 143.97, 142.85, 139.72, 138.67, 137.06, 129.88, 127.02, 125.05, 119.97, 114.80, 114.18, 113.62, 68.14, 63.81, 31.66, 29.29, 25.75, 22.59, 14.03. Anal. Calcd: C, 69.28; H, 4.82; N, 3.44. Found: C, 69.62; H, 4.65; N, 3.37.

Table S1. Molecular weights and thermal properties of the polymers and small molecule.

Material	$M_{\mathrm{n}}^{\mathrm{a}}$	$M_{\mathrm{w}}^{\mathrm{a}}$	PDI$^{\mathrm{a}}$	$T_{\mathrm{d}}^{\mathrm{b}}$
BO2FC8	31.5k	71.2k	2.3	314
BO2FEH	25.2k	53.6k	2.1	300
m-ITIC-OR-4Cl	–	–	–	325

a: Values of M_{n}, M_{w}, and PDI of the polymers were determined through gel permeation chromatography (GPC) in dichlorobenzene, using polystyrene standards. b: 5% Weight loss temperature (°C) in air.

Table S1 lists the molecular weights and thermal properties of the two synthesized polymers, with the different side chains, and the thermal properties of the small molecule. The molecular weight of BO2FC8 was higher than that of BO2FEH; because branched side chains have steric bulk greater than that of linear side chains, we suspect that a higher ratio of branched chains would be slightly harder to polymerize. Consistent with our previous findings,[5] fluorine-substituted polymeric structures typically have lower molecular weights because their stronger intermolecular interactions lower their solubility, thereby hindering the polymerization process.

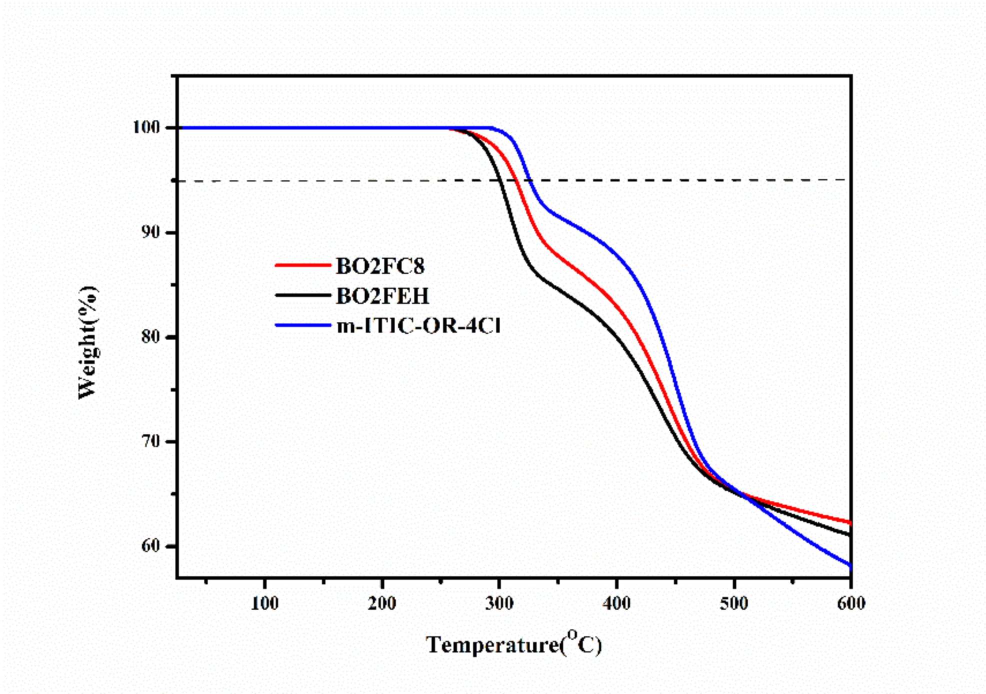

Fig. S1 TGA thermograms of BO2FC8, BO2FEH, and m-ITIC-OR-4Cl, recorded at a heating rate of 10 °C min^{-1} under a N_2 atmosphere.

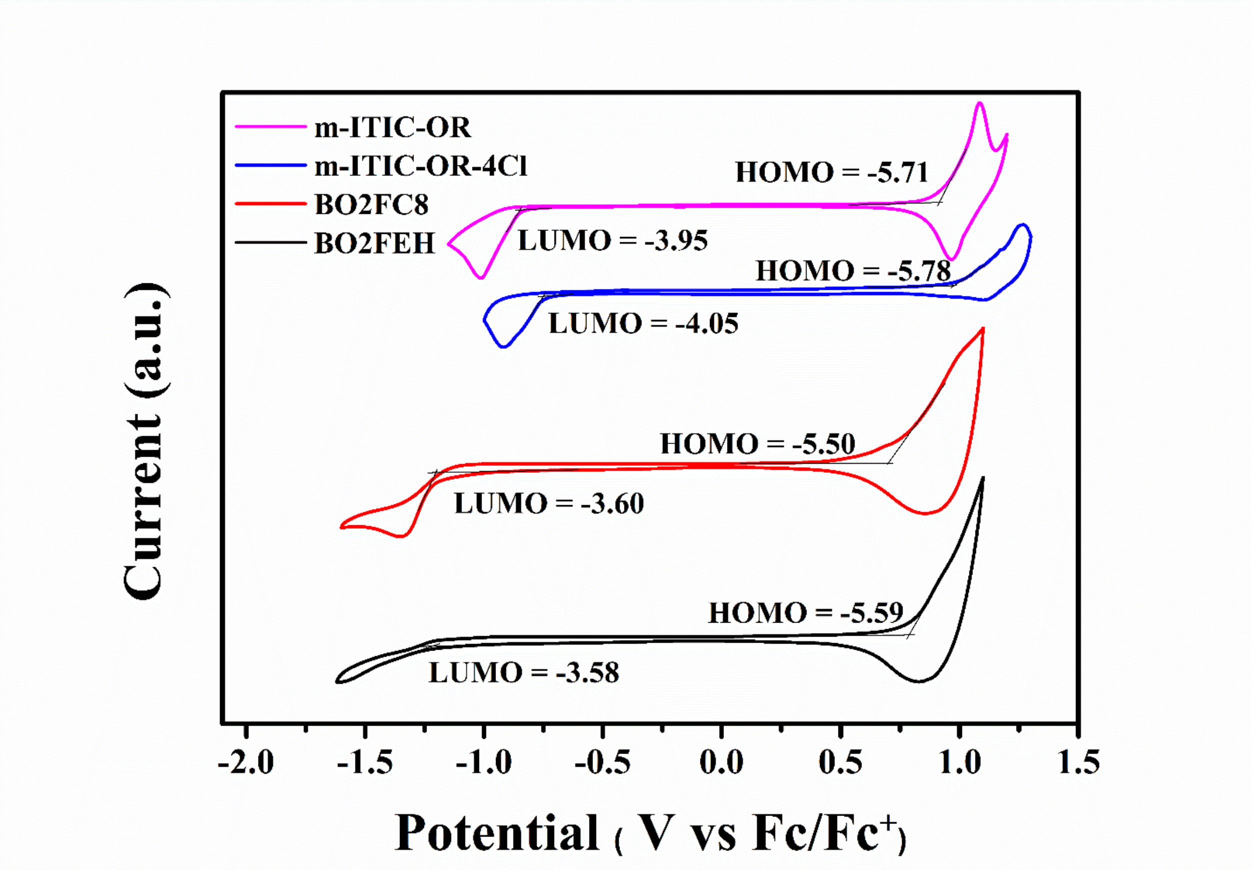

Fig. S2 Cyclic voltammograms of m-ITIC-OR, m-ITIC-OR-4Cl, and the isomeric polymers as solid films.

Table S2. Optical and electrochemical properties of the materials.

	E_{onset}^{ox} (V)	E_{onset}^{red} (V)	LUMO^{CV} (eV)	HOMO^{CV} (eV)	E_g^{ec}(eV)	λ_{onset} (nm)	E_g^{opt} (eV)
BO2FC8	0.70	–1.20	–3.60	–5.50	1.90	700	1.77
BO2FEH	0.79	–1.22	–3.58	–5.59	2.01	687	1.80
m-ITIC-OR-4Cl	0.98	–0.75	–4.05	–5.78	1.73	816	1.52

Table S3. Parameters used in random forest algorism to predict the PCE.

	Chemical structure	**Mw**	**HOMO (eV)**	**E_g^{ec}(eV)**
BO2FC8	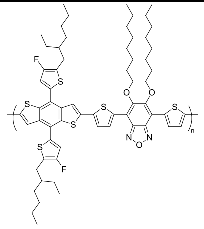	71.2k	–5.50	1.90
BO2FEH	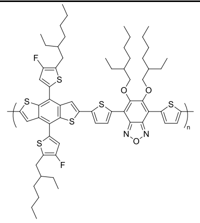	53.6k	–5.59	2.01
m-ITIC-OR-4Cl	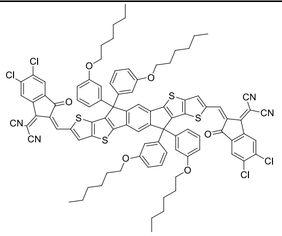	1629.7	–5.78	1.73

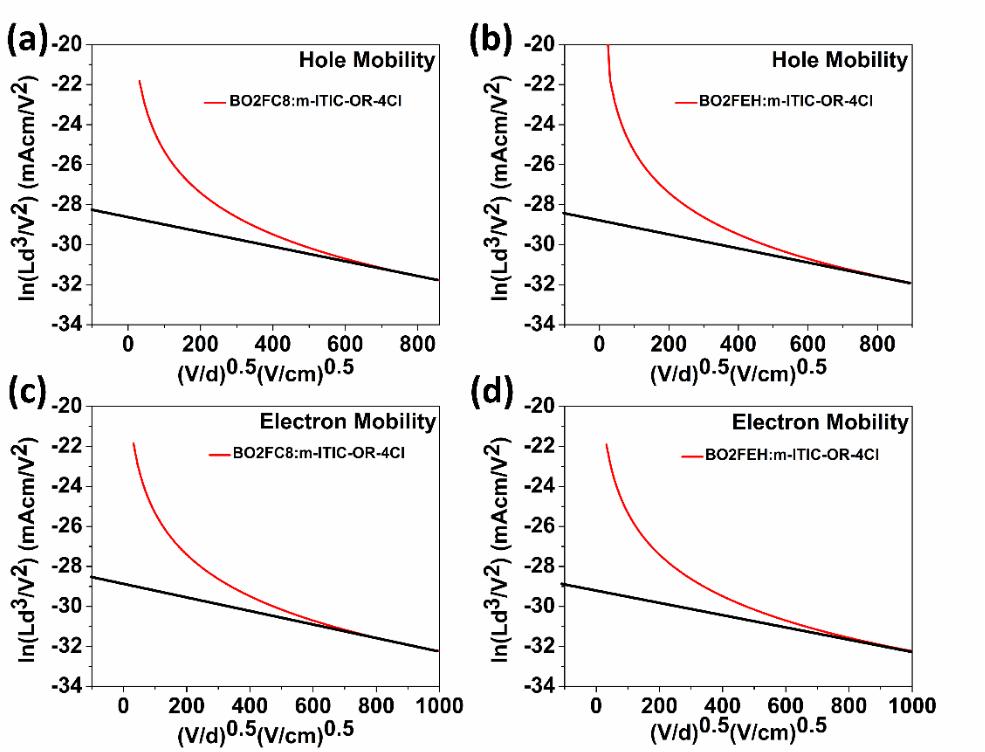

Fig. S3 (a, b) Hole-only and (c, d) electron-only devices based on BO2FC8:m-ITIC-OR-4Cl and BO2FEH:m-ITIC-OR-4Cl blend films.

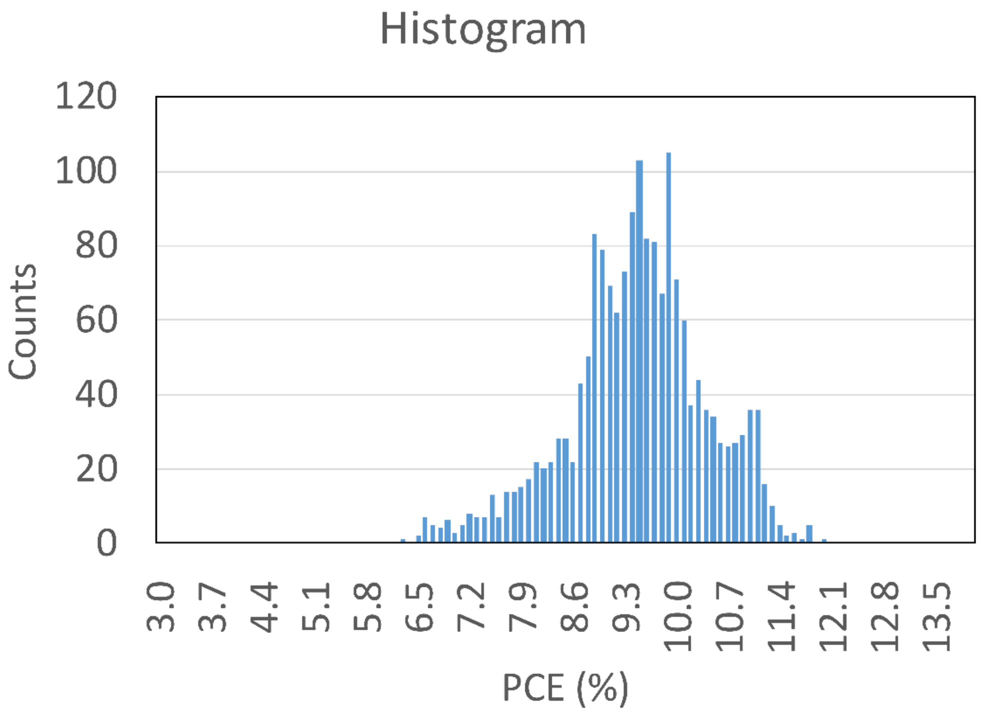

Fig. S4 Histogram of polymer:m-ITIC-OR-4Cl screening (~1700).

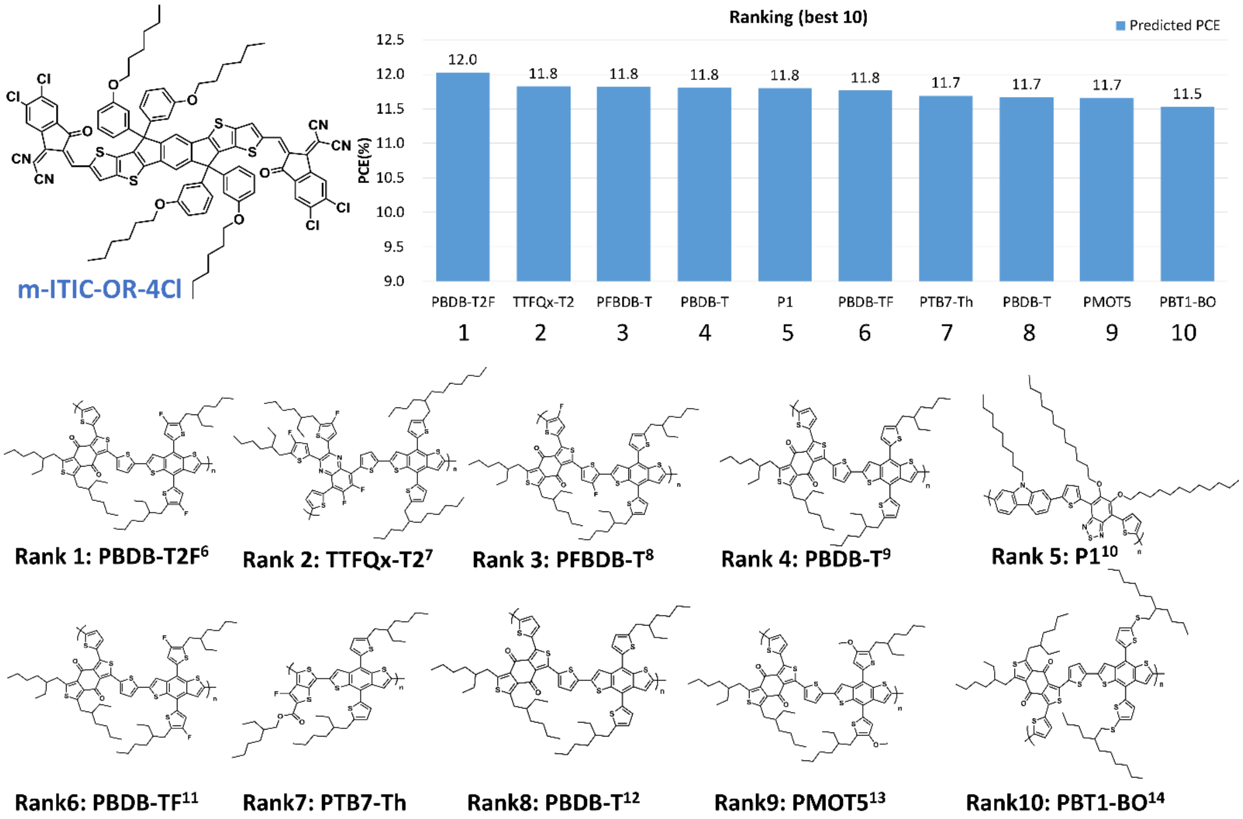

Rank 1: PBDB-T2F[6] **Rank 2: TTFQx-T2**[7] **Rank 3: PFBDB-T**[8] **Rank 4: PBDB-T**[9] **Rank 5: P1**[10]

Rank6: PBDB-TF[11] **Rank7: PTB7-Th** **Rank8: PBDB-T**[12] **Rank9: PMOT5**[13] **Rank10: PBT1-BO**[14]

Fig. S5 Polymer screening (~1700) suitable for m-ITIC-OR-4Cl.[6-14]

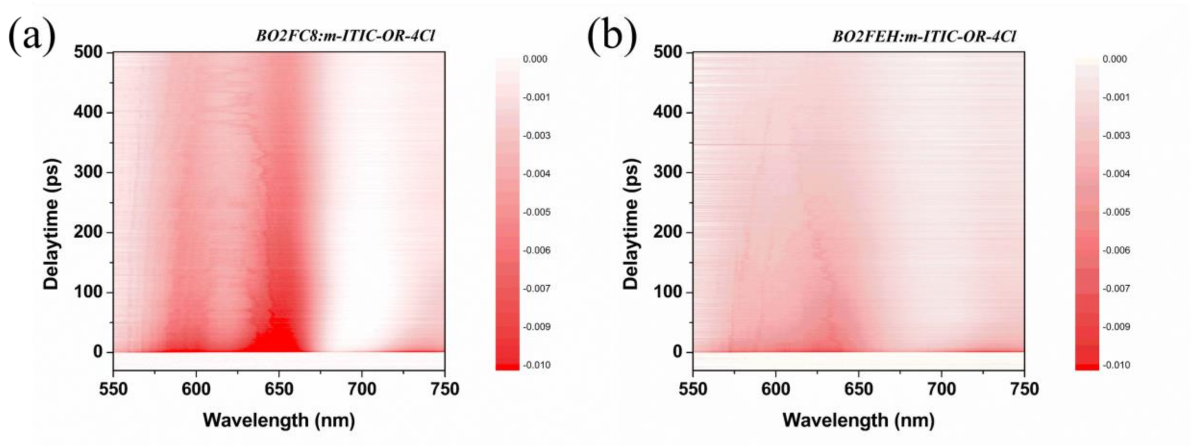

Fig. S6 2-D plots of the ultrafast transient absorption differences (ΔA) of the (c) BO2FC8:m-ITIC-OR-4Cl and (d) BO2FEH:m-ITIC-OR-4Cl blends.

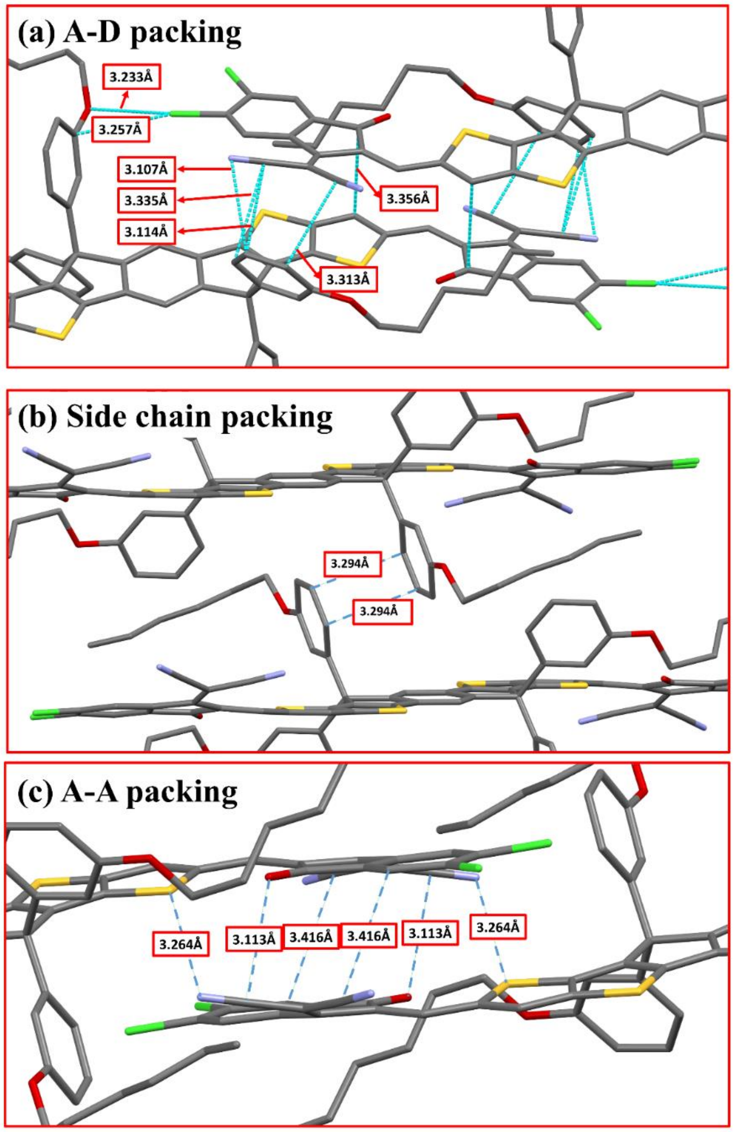

Fig. S7 Packing distances of (a) A-D, (b) side chain, and (c) A-A mode.

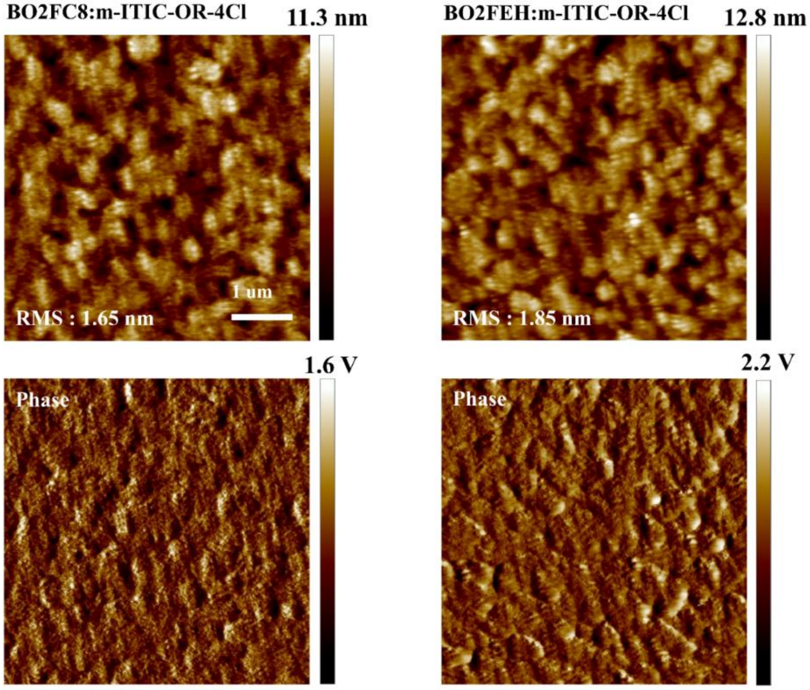

Fig. S8 AFM height and phase images (5 × 5 μm) images of BO2FC8:m-ITIC-OR-4Cl and BO2FEH:m-ITIC-OR-4Cl films.

To obtain insight into their morphologies, we recorded atomic force microscopy (AFM) images of the two blend films (Figure S4). The height images revealed that, when incorporated in small molecule blends, the miscibility of the polymer donor and small-molecule acceptor was improved, thereby resulting in smooth surfaces with low root-mean-square (rms) surface roughnesses: 1.65 and 1.85 nm for BO2FC8:m-ITIC-OR-4Cl and BO2FEH:m-ITIC-OR-4Cl films, respectively. We suspect that the smaller rms roughness and the more uniform phase image of the BO2FC8:m-ITIC-OR-4Cl film resulted from superior aggregation of the linear side chains, thereby enhancing the film-forming properties and improving the packing of the active layer blend into a more compact film. Figure S5 displays transmission electron microscopy (TEM) images of the BO2FC8:m-ITIC-OR-4Cl and BO2FEH:m-ITIC-OR-4Cl films; any differences between the two are difficult to distinguish since both polymer and small molecule have about the same electron density.

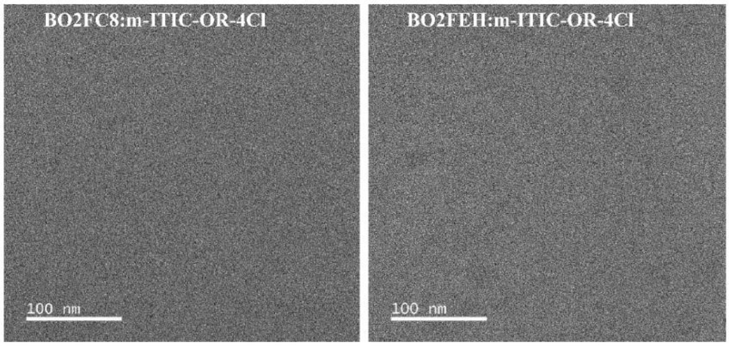

Fig. S9 TEM images of BO2FC8:m-ITIC-OR-4Cl and BO2FEH:m-ITIC-OR-4Cl films.

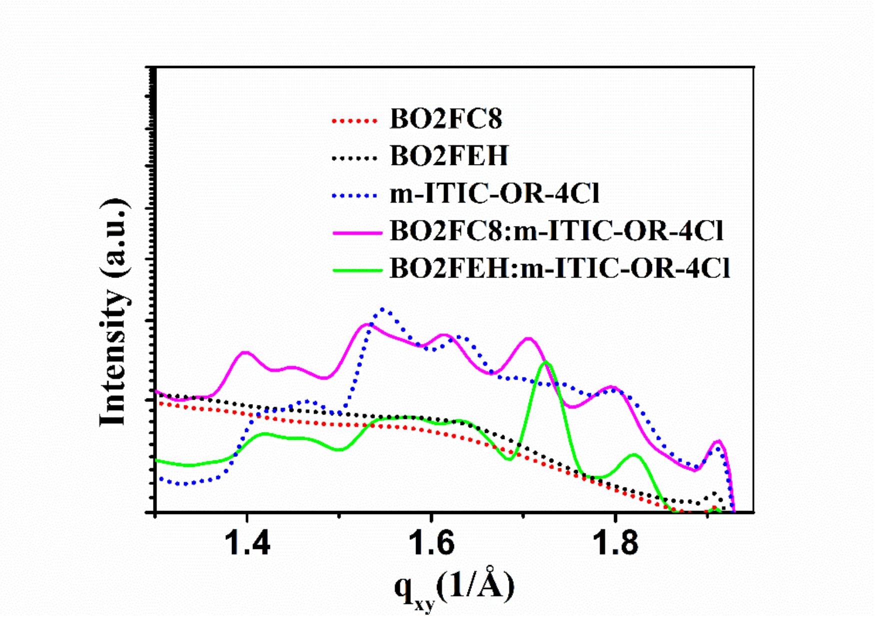

Fig. S10 Corresponding 1-D GIWAXS profiles of m-ITIC-OR-4Cl, BO2FC8, and BO2FEH and the binary blends BO2FC8:m-ITIC-OR-4Cl and BO2FEH:m-ITIC-OR-4Cl, reduced from the in-plane directions.

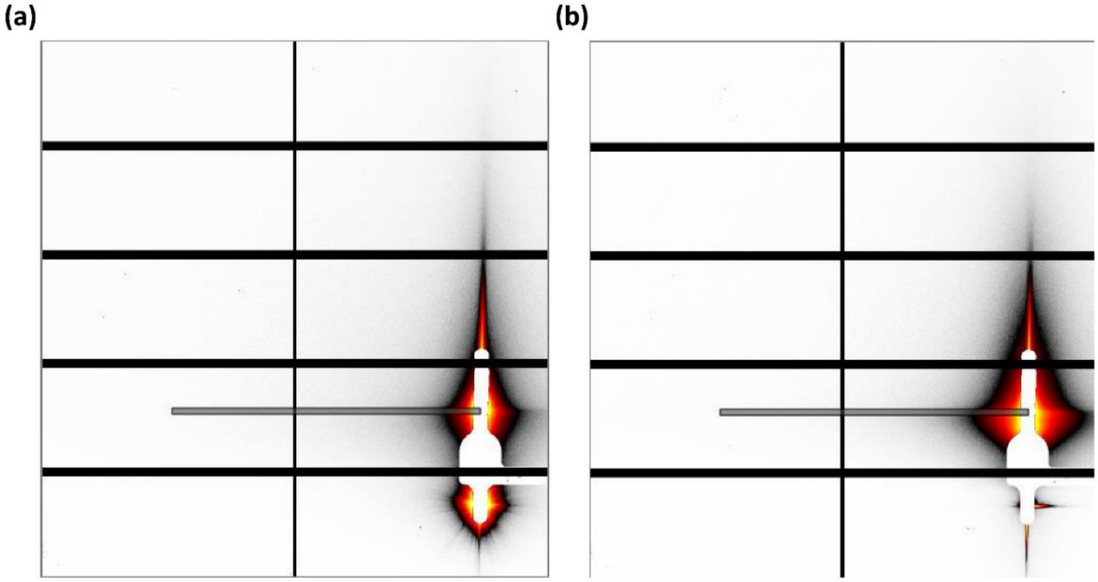

Fig. S11 GISAXS images of BO2FC8:m-ITIC-OR-4Cl and BO2FEH:m-ITIC-OR-4Cl films.

Table S4. Fitting parameters obtained from the GISAXS curves of the binary blend films (Model: Cylinder - Polydisperse Length)

Composition	BO2FC8:m-ITIC-OR-4Cl	BO2FEH: m-ITIC-OR-4Cl
Scale	0.121924	0.083722
Radius (Å)	833.766	746.545
Length (Å)	29.5127	54.5451
Polydispersity of length	0.00123776	0.309568
SLD cylinder (Å^{-2})	1×10^{-6}	1×10^{-6}
SLD solvent (Å^{-2})	1.06791×10^{-6}	9.06226×10^{-7}
Incoh. bkg (cm^{-1})	0.00103657	0.000826549

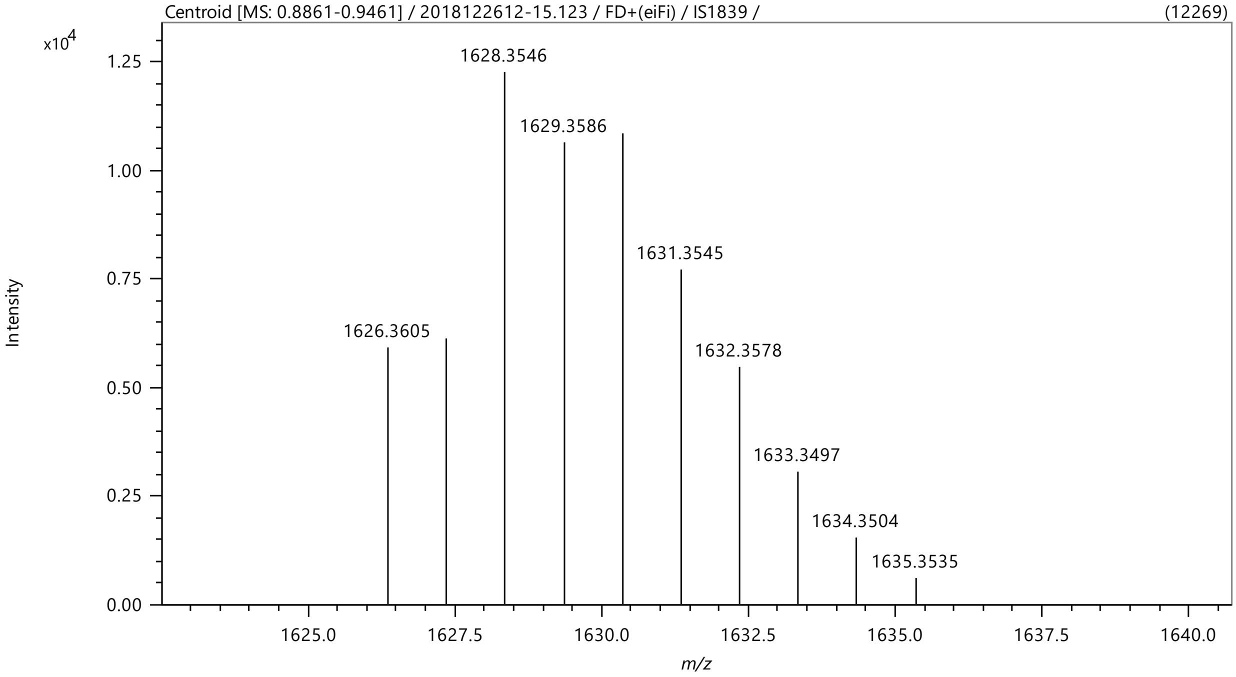

Fig. S12 High resolution field desorption mass spectroscopy of m-ITIC-OR-4Cl.

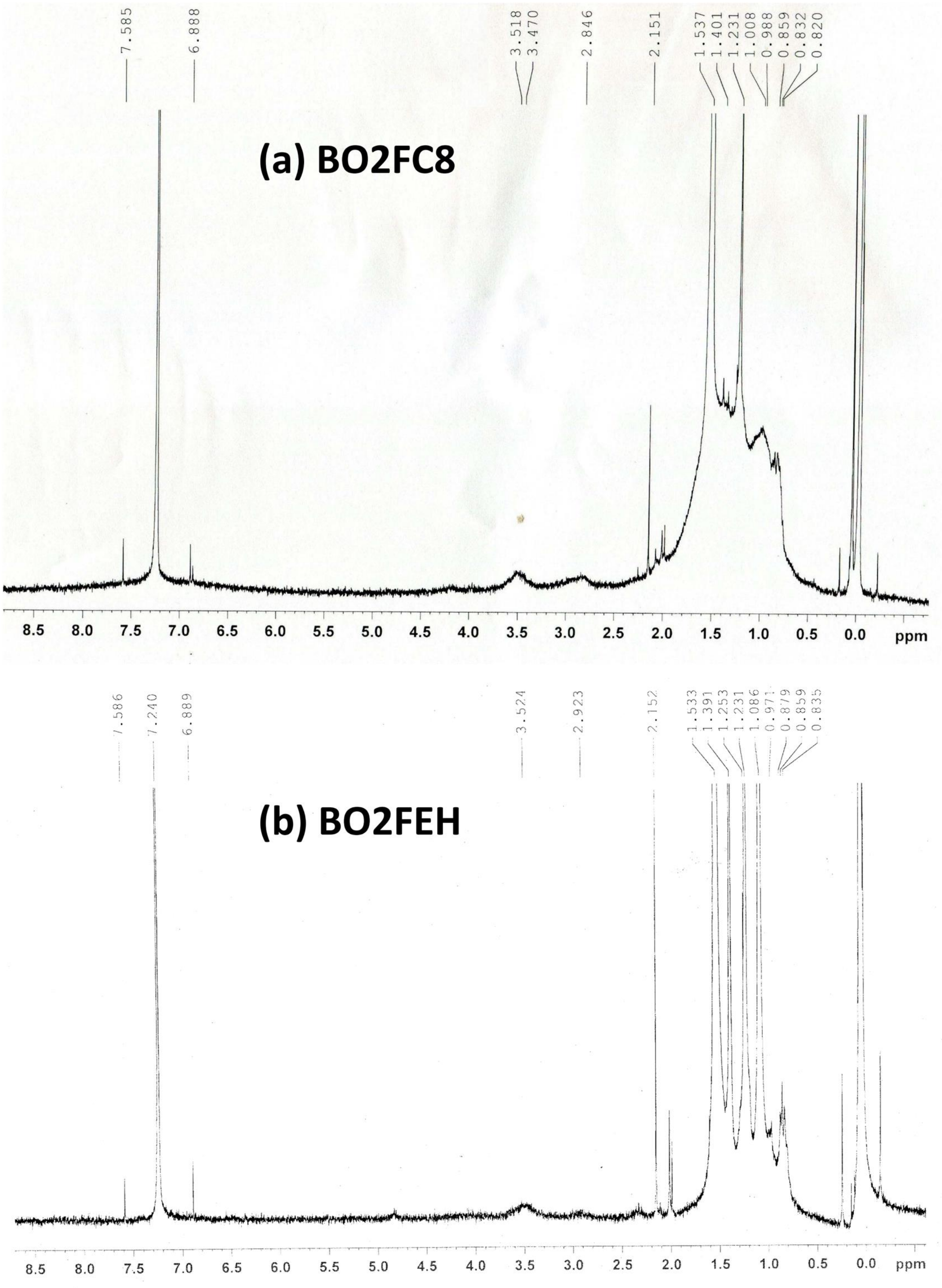

Fig. S13 ^{1}H NMR of (a) BO2FC8 and (b) BO2FEH.

Machine Learning

The PCE prediction of polymer:small molecule acceptor (SMA) solar cell was performed by machine learning based on random forest algorism according to the same procedure in the previous report.[15] Modelings were performed on a notebook computer using R studio (a free software, https://www.rstudio.com/). Experimental polymer:SMA data (~500 data) including each device parameters (PCE, J_{sc}, V_{oc}, and FF) and material properties (chemical structure, weight-averaged molecular weight: M_w, HOMO level, and bandgap: E_g) were collected from the literature and used as the training data. The PCEs of the two new polymers with the SMA were predicted using their chemical fingerprints (ECFP6 key, identical to Morgan fingerprint), as calculated from the chemical structures, M_w of the polymer, molecular weight of SMA, HOMO levels of polymer and SMA, E_gs of polymer and SMA as the explanatory variables.

Measurements and Characterization

Thermogravimetric analysis (TGA) was performed using a TA Instruments Q500 apparatus; the thermal stabilities of the samples were controlled under a N_2 atmosphere by measuring their weight losses while heating at a rate of 10 °C min^{-1}. ^{1}H NMR spectra were recorded using a Varian UNITY 300 MHz spectrometer. UV–Vis spectra of solid films, spin-coated from polymer solutions onto a quartz substrate, were recorded using a Hitachi U-4100 spectrophotometer. PL spectra were recorded using a HITACHI F-4500. Samples were prepared by spin-casting CB solutions onto silicon substrates; the thickness was maintained at approximately 100 nm. Cyclic voltammetry (CV) of the polymer films was performed using a BAS 100 electrochemical analyzer operated at a scan rate of 50 mV s^{-1}; the solvent was anhydrous MeCN, containing 0.1 M tetrabutylammonium hexafluorophosphate ($TBAPF_6$) as the supporting electrolyte. The potentials were measured against a Ag/Ag^+ (0.01 M $AgNO_3$) reference electrode, using the ferrocene/ferrocenium ion (Fc/Fc^+) pair as the internal standard (0.09 V). The onset potentials were determined from the crossing of two tangents drawn at the increasing and background currents of the cyclic voltammograms. HOMO energy levels were estimated relative to the energy level of the ferrocene reference (4.8 eV below vacuum level). Topographic and phase images of the polymer:m-ITIC-OR-4Cl films (surface area: 5×5 μm^2) were recorded using a Digital Nanoscope III atomic force microscope operated in tapping mode under ambient conditions. The thickness of the active layer of the device was measured using a VeecoDektak 150 surface profiler. GIWAXS/GISAXS was performed at the 23A beamline (10 keV) of the National Synchrotron Radiation Research Center (NSRRC), Hsinchu, Taiwan, using a 0.2° incident angle. Samples were prepared by spin-casting CB solutions of PBDTTBO-2F isomer:m-ITIC-OR-4Cl blends onto silicon substrates, the thickness were maintained around 100 nm. GIWAXS/GISAXS experiments were conducted after the solvent had evaporated entirely.

Fabrication and Characterization of Photovoltaic Devices

Zinc acetate dihydrate [$Zn(CH_3COO)_2{\cdot}2H_2O$] (1.0 g) and ethanolamine (0.28 g) were dissolved in 2-methoxyethanol (10 mL) under dynamic stirring for 12 h. Mixture solutions of the active layers were set by dissolving the isomeric polymers (6 mg mL^{-1}) and m-ITIC-OR-4Cl (9 mg mL^{-1}) in CB, resulting in a total concentration of 1.5 wt%. The mixture solutions were stirred uninterruptedly in a glove box for 12 h at 90 °C to ensure complete dissolution of the isomeric polymers and m-ITIC-OR-4Cl. Indium tin oxide (ITO)–coated glass substrates (5 Ω cm^{-2}, Merck) were rinsed through sequential ultrasonication with detergent, acetone, DI water, and isopropanol (20 min each) and then dried under a flow of N_2. ZnO was spin-coated onto the UV ozone-treated ITO for 15 min and then annealed at 200 °C for 1 h. To prepare the PEI-doped electron transport layer, the zinc oxide solution was mixed dynamically with 5% of PEI (branched; average M_n = ca. 10k; Sigma–Aldrich) for 12 h, as described previously.[16] The substrates were transferred to a dry N_2–filled glove box. The ZnO layers were placed at a thickness of nearly 40 nm, followed by accumulation of the active layers. The active layers, formed from PBDTTBO-2F isomer:m-ITIC-OR-4Cl blend solutions in CB, were prepared in a glove box and then spin-cast on top of the ZnO films. After the CB in the films had evaporated, the films were heated at 150 °C for 10 min. The PBDTTBO-2F isomer:m-ITIC-OR-4Cl blend films were then covered with Petri dishes for 20 min prior to deposition of the anode. The active layers of PBDTTBO-2F isomer:m-ITIC-OR-4Cl blends had thicknesses of roughly 100 nm. The BHJ devices were fabricated with structures incorporating ITO/ZnO. Device fabrication was complete after thermal evaporation of the P-type material (MoO_3, 10 nm) and the anode (Ag, 100 nm) under high vacuum (ca. 10^{-7} torr). A shadow mask was used during the thermal evaporation procedure to define a device area of 0.1 cm^2.

The current density–voltage (J–V) characteristics were measured using a Keithley 2400 source meter. The photocurrent was measured under simulated AM 1.5 G illumination at 100 mW cm^{-2} using a Xe lamp–based Newport 150-W solar simulator. A calibrated Si photodiode with a KG-2 filter was employed to confirm the illumination intensity. EQEs were measured using an SRF50 system (Optosolar, Germany). A calibrated mono-silicon diode exhibiting a response at 300–800 nm was used as a reference. For measurements of hole and electron mobilities, devices were fabricated having the structure ITO/PEDOT:PSS/binary blend/silver (Ag) and ITO/ZnO/binary blend/Ca/Al, individually. Hole-only or electron-only diodes were fabricated using the following architectures: ITO/PEDOT:PSS/active layer/Ag for holes and aluminium (Al)/active layer/Al for electrons. J-V characteristics of these diodes were taken under dark in glove box with a nitrogen atmosphere. Mobilities were extracted by fitting the current density-voltage curves using the Mott-Gurney relationship (space charge limited current).

Transient Absorption Spectroscopy

Time-resolved pump-probe studies were performed using a femtosecond Ti:sapphire laser system (Legend-USP-HP, Coherent) delivering a near-infrared (NIR) pulse (duration: ca. 40 fs; repetition rate: 5 kHz; center wavelength: 800 nm). The NIR laser pulse was split into two NIR pulses, with a power ratio of 10:1, using a beam splitter. The higher-intensity NIR pulse was focused into a β-barium borate crystal for second harmonic (SH) generation; the generated SH laser pulse was guided to a delay stage for retro reflection, and then focused onto the sample as a pump pulse. The lower-intensity NIR pulse (pulse energy: 5 μJ) was focused onto a sapphire plate (thickness: 2 mm) to generate a white light continuum (WLC); the WLC pulse was focused onto the sample as a WLC probe pulse. Using a parabolic mirror, both the pump (400 nm) and WLC probe (500–750 nm) pulses were focused onto the sample. A charge-coupled device camera (Series 2000, Entwicklungsburo Stresing), connected through an optical fiber and polychromator (CP140, Yobin Yvon), recorded the probe pulse transmitted through the sample. For measurements of the change in absorption with and without sample excitation, the pump frequency was modulated with an optical chopper running at 2.5 kHz. The difference absorption spectrum (ΔA) of the sample at each time delay between the pump and probe pulses was acquired using LabVIEW software. The delay was scanned using a delay stage inserted in the optical path of the pump pulses.

References

(1) J. M. Jiang, H. K. Lin, Y. C. Lin, H. C. Chen, S. C. Lan, C. K. Chang, K. H. Wei, *Macromolecules*, 2014, **47**, 70–78.

(2) M. Zhang, X. Guo, S. Zhang, J. Hou, *Adv. Mater.*, 2014, **26**, 1118–1123.

(3) Z. Zhang, L. Feng, S. Xu, Y. Liu, H. Peng, Z. G. Zhang, Y. Li, Y. Zou, *Adv. Sci.*, 2017, **4**, 1700152.

(4) Y. Cui, C. Yang, H. Yao, J. Zhu, Y. Wang, G. Jia, F. Gao, J. Hou, *Adv. Mater.*, 2017, **29**, 1703080.

(5) Y. C. Lin, H. W. Cheng, Y. W. Su, B. H. Lin, Y. J. Lu, C. H. Chen, H. C. Chen, Y. Yang, K. H. Wei, *Nano Energy*, 2018, **43**, 138–148.

(6) H. Zhang, H. Yao, J. Hou, J. Zhu, J. Zhang, W. Li, R. Yu, B. Gao, S. Zhang, J. Hou, *Adv. Mater.*, 2018, **30**, 1800613.

(7) S. Xu, X. Wang, L. Feng, Z. He, H. Peng, V. Cimrová, J. Yuan, Z.-G. Zhang, Y. Li, Y. Zou, *J. Mater. Chem. A*, 2018, **6**, 3074–3083.

(8) Z. Fei, D. F. Eisner, X. Jiao, M. Azzouzi, J. A. Röhr, Y. Han, M. Shahid, A. S. R. Chesman, C. D. Easton, C. R. McNeill, T. D. Anthopoulos, J. Nelson, M. Heeney, *Adv. Mater.*, 2018, **30**, 1705209.

(9) Y. Nian, F. Pan, S. Li, H. Jiang, S. Feng, L. Zhang, Y. Cao, J. Chen, *Asian J. Org. Chem.*, 2018, 10.1002/ajoc.201800389.

(10) J. Zhang, X. Zhang, G. Li, H. Xiao, W. Li, S. Xie, C. Li, Z. Bo, *Chem. Commun.*, 2016, **52**, 469–472.

(11) S. Li, L. Zhan, W. Zhao, S. Zhang, B. Ali, Z. Fu, T.-K. Lau, X. Lu, M. Shi, C.-Z. Li, J. Hou, H. Chen, *J. Mater. Chem. A*, 2018, **6**, 12132–12141.

(12) W. Gao, M. Zhang, T. Liu, R. Ming, Q. An, K. Wu, D. Xie, Z. Luo, C. Zhong, F. Liu, F. Zhang, H. Yan, C. Yang, *Adv. Mater.*, 2018, **30**, 1800052.

(13) W. Huang, M. Li, L. Zhang, T. Yang, Z. Zhang, H. Zeng, X. Zhang, L. Dang, Y. Liang, *Chem. Mater.*, 2016, **28**, 5887–5895.

(14) T. Liu, X. Pan, X. Meng, Y. Liu, D. Wei, W. Ma, L. Huo, X. Sun, T. H. Lee, M. Huang, H. Choi, J. Y. Kim, W. C. H. Choy, Y. Sun, *Adv. Mater.*, 2017, **29**, 1604251.

(15) S. Nagasawa, E. Al-Naamani, A. Saeki, *J. Phys. Chem. Lett.*, 2018, **9**, 2639–2646.

(16) H. C. Chen, S. W. Lin, J. M. Jiang, Y. W. Su, K. H. Wei, *ACS Appl. Mater. Interfaces*, 2015, **7**, 6273–6281.